Forcing dependence of atmospheric lapse rate changes dominates residual polar warming in solar radiation management scenarios.

Matthew Henry[1]and Timothy M. Merlis[1]

[1]Department of Atmospheric and Oceanic Sciences, McGill University, Montreal, Quebec, Canada.

Corresponding author: Matthew Henry, matthew.henry@mail.mcgill.ca

Abstract

Solar radiation management (SRM) geoengineering has been proposed as a way of counteracting the warming effects of increasing greenhouse gases by reflecting solar radiation [6]. Simulations using comprehensive general circulation models (GCM) show a residual surface warming at the poles when the solar constant is reduced to balance the global mean surface temperature change from increased carbon dioxide (CO_2) concentration [20]. Previous work attributes this residual warming to the difference in forcing structure between the increase in greenhouse gases and the decrease in solar insolation [6]. However, the atmospheric energy transport convergence near the poles is also reduced, so that the total energy input to the high latitudes is small [19]. Here we show that the forcing dependence of the high latitude lapse rate change induces a bottom-heavy temperature change and explains how even a small energy input can induce residual polar warming. An idealized atmospheric GCM with aquaplanet boundary condition, no sea ice or clouds is shown to reproduce the temperature and atmospheric energy transport change from comprehensive GCMs. A single column model (SCM) is then used to decompose the total high latitude temperature change into the effects of the CO_2 increase, the insolation decrease, and the atmospheric energy transport change separately. The SCM enables the computation of the temperature change associated with each forcing and feedback. It is used to show that the combination of the bottom-heavy warming from increased CO_2 and the more vertically homogeneous cooling from insolation and energy transport changes induce a very bottom-heavy temperature change. An analytic model of the high-latitude atmosphere is then used to reason about the forcing dependence of lapse rate changes for an atmosphere in radiative-advective equilibrium [2]. This model hierarchy invites a more careful analysis of attributions of high latitude surface temperature changes to the lapse rate feedback, as it has distinct responses to various forcings and nonlocal processes.

Proposed solar radiation management (SRM) geoengineering schemes aim to cool the Earth to counteract the radiative forcing and warming from anthropogenic emissions. Injecting sulphate aerosols or their precursors in the stratosphere is one widely discussed SRM geoengineering technique, and climate model simulations of it have similar tropospheric temperature changes when compared with the idealization of reducing the solar constant [11]. The experiment G1 of the Geoengineering Model Intercomparison Project (GEOMIP) consists of reducing the solar constant to compensate for abruptly quadrupled CO_2 concentrations in fully coupled general circulation models (GCM) [12]. In the G1 experiments, a residual polar warming occurs: the surface air temperature change is positive near the poles and slightly negative in the tropics [20]. Figure 1a and 1c show the atmospheric and surface temperature change respectively between the geoengineered G1 experiment and preindustrial control climate from five comprehensive climate models (listed in legend of figure 1c). While there is a slight surface cooling in the tropics, the high latitudes of both hemispheres have from 0.5K to 2K of residual warming. This residual polar warming has important consequences for the shift in the intertropical convergence zone (ITCZ) and changes in atmospheric energy transport in solar geoengineered climates [19]. It is also relevant to our understanding of the polar amplification of surface temperature change and vertical structure of temperature change under increased CO_2 [14;17;8].

This residual polar warming is commonly explained by the difference in latitudinal forcing structure between the increase in greenhouse gases and the decrease in solar insolation, which leads to a positive top-of-atmosphere (TOA) forcing at the poles, a negative TOA forcing in the tropics, and a near-zero global-mean TOA forcing [6]. The tropically-amplified CO_2 forcing results from the climatological atmospheric lapse rate being larger in the tropics than near the poles [9] and is more latitudinally homogeneous than the forcing from reduced insolation [7]. This explanation, however, does not account for changes in atmospheric energy transport that result from latitudinally inhomogeneous TOA forcing. In Merlis & Henry [15], we compute an analytic estimate of the effect of the

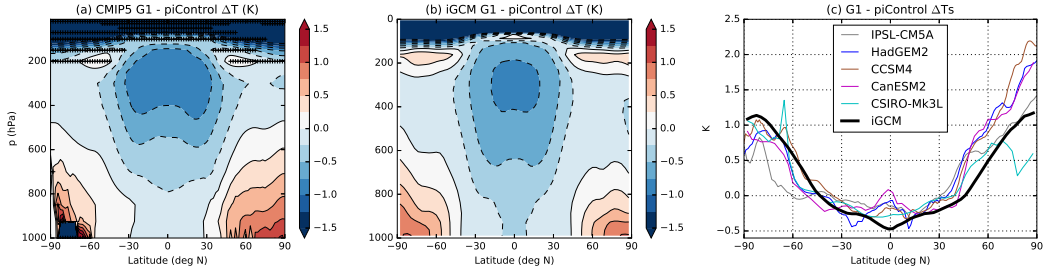

Figure 1. Residual polar warming occurs in climate model simulations of SRM geoengineering. Temperature change between the solar geoengineered simulation (G1) and the preindustrial control simulation (piControl) from (a) mean of 5 CMIP5 models (IPSL CM5A, HadGEM2, CCSM4, CanESM2, CSIRO-Mk3L) and (b) idealized GCM. Crosses in (a) indicate regions where the standard deviation is larger than 1.5. (c) Surface temperature changes from the 5 CMIP5 models (colors) and the idealized GCM (black).

different latitudinal structure of the solar and CO_2 forcings on the surface air temperature change in geoengineered climates that includes the effect of energy transport: we find that this effect accounts for approximately half of the total residual polar warming in the absence of regional climate feedback mechanisms.

The vertical structure of atmospheric temperature change is top-heavy in the tropics and bottom-heavy in the poles (figure 1a). In the tropics, the atmosphere is close to radiative-convective equilibrium: radiative cooling is balanced by convective heating. The vertical structure of temperature is approximately determined by the moist adiabat, hence the lapse rate is uniquely a function of surface temperature and relative humidity. Therefore, the lapse rate change depends only on the surface temperature change, assuming no change in relative humidity [21]. Near the poles, however, the atmosphere is close to "radiative-advective" equilibrium: warming from atmospheric energy transport is balanced by radiative cooling. Cronin & Jansen [2] use an analytic radiative-advective model of the high latitude atmosphere to show that the lapse rate response differs depending on the nature of the forcing. In their model, a positive surface forcing (e.g., an increase in convergence of ocean heat transport or absorbed solar radiation at the surface) induces a destabilizing lapse rate change, a positive longwave radiative forcing induces a more destabilizing lapse rate change than the surface forcing, and an increase in atmospheric energy transport and/or solar atmospheric heating induces a weakly stabilizing or neutral lapse rate change. Moreover, they suggested that each additional feedback such as water vapor, clouds, or surface albedo would induce a different lapse rate response. While this simple model lead to the important insight that the high-latitude lapse rate change is forcing-dependent, the simple treatment of atmospheric energy transport results in a vertically uniform temperature change, whereas it has been suggested to preferentially affect the mid-troposphere in comprehensive climate models [13]. For SRM perturbations, we expect the CO_2 forcing to have a more bottom-heavy temperature response than the reductions in solar forcing and atmospheric energy transport, leading to a meaningful surface temperature response for a small total forcing. In this paper, we quantify the contributions of forcings and feedbacks to the total high latitude lapse rate change and concommitant surface temperature change in the solar radiation management experiment.

We implement a SRM experiment using an idealized atmospheric GCM. A version of the Geophysical Fluid Dynamics Laboratory (GFDL) atmospheric GCM is used with no clouds, comprehensive clear-sky radiation, annual-mean insolation, and aquaplanet surface boundary conditions with no sea ice. In order to compensate for the cooling ra-

diative effect of clouds, the surface albedo is set to be an approximation of Earth's TOA albedo (figure S1). The control simulation has a CO_2 concentration of 300ppm and the solar constant is 1365 $W\,m^{-2}$. The solar constant in the SRM run is decreased to 1317 $W\,m^{-2}$ (a 3.5% reduction) in order to get zero-mean surface air temperature change when the CO_2 concentration is quadrupled. More details on the model are given in Methods.

Figure 1b shows the atmospheric temperature change between the control and SRM idealized GCM simulations, which has a similar structure to that of comprehensive GCMs (figure 1a). The surface temperature change between the control and SRM run in the idealized GCM (black) is also reasonably close to the comprehensive GCMs (figure 1c). In addition, the change in atmospheric energy transport is similar to that of comprehensive GCMs (a reduction of 0.1 PW in midlatitudes, figure S3b and figure 1 of Russotto & Ackerman[19]). This model's ability to reproduce the temperature and atmospheric energy transport changes from comprehensive GCM simulations suggest that processes present in this idealized model are sufficient to explain the ensemble-mean changes in SRM experiments. The idealized GCM underestimates the Arctic surface temperature change from comprehensive GCMs, which is consistent with the absence of sea ice albedo feedback in the idealized GCM. We proceed to decompose the high-latitude temperature response in this GCM to identify the mechanism responsible for residual polar warming.

To decompose the high-latitude temperature change in the idealized GCM simulation, we use a single column model (SCM) of the high latitudes where the insolation, CO_2 concentration, atmospheric energy transport, and specific humidity profile are inputs. We use a python package for process-oriented climate modeling called climlab[18]. Values from the idealized GCM experiments averaged poleward of 80°N are used to prescribe the specific humidity profile, which affects the radiation and surface latent heat flux. In addition, the time-mean advection and condensation temperature tendency profiles from GCM simulations are added as an external temperature tendency term to simulate atmospheric energy transport. Since the atmospheric energy transport induces a stable temperature structure, running the model with convection yields the same results. This is a column model of the high latitudes, hence we consider the prescribed atmospheric energy transport to be a "forcing" in this context. The climatological polar temperatures of the idealized GCM and SCM are similar (figure S4).

We run four simulations: quadrupled CO_2, reduced insolation, perturbed energy transport, and a simulation with all perturbations ($4xCO_2$ and reduced insolation, energy transport, and specific humidity). The separation of individual perturbations in the SCM assumes the full response to SRM is comprised of the linear superposition of these changes. Superposition holds precisely in the SCM, and largely in the idealized GCM, except for a $\approx 10\%$ in the global mean (figure S2).

Figure 2a shows that the idealized GCM's vertical temperature change structure in high latitudes (black, "iGCM") is similar to that of five CMIP5 models in the Arctic (colors, listed in legend). Figure 2b shows the temperature change structure for the different SCM simulations, with points showing surface (or skin) temperature changes. The CO_2-only simulation ("CO_2", red) has a bottom-heavy temperature change structure and a surface temperature increase of 3.1K. The insolation reduction simulation ("Solar", yellow) has a more vertically uniform cooling structure and a surface temperature change of -1.5K. The energy transport change ("ET", green) preferentially cools the lower atmosphere and leads to a -0.5K surface temperature change. Finally, when all perturbations (CO_2, insolation, water vapor and energy transport) are included ("All", black), the surface temperature change is 1.1K, as was simulated by the idealized GCM (1.1K). The differences between the comprehensive GCMs (figure 2a, colors), the idealized GCM (figure 2a, black), and the SCM (figure 2b, black) can be due to the different radiation schemes, to the time-averaging of boundary conditions in the SCM, and to the absence of climate components such as clouds, sea ice, and ocean circulation.

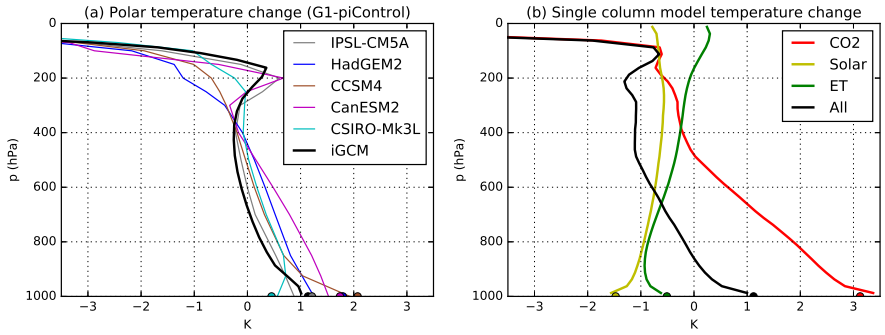

Figure 2. Residual warming arises from bottom-heavy CO_2 warming, while solar forcing and atmospheric energy transport changes have more uniform cooling. (a) Temperature difference between solar geoengineered simulation (G1) and control simulation (piControl) in the Arctic (>80° North) for the idealized GCM (black) and comprehensive GCMs (colors, listed in legend). (b) Decomposition of polar temperature change using the single column model: increased CO_2 (red), reduced insolation (yellow), decreased energy transport (green), and all perturbations (black).

Run name	ΔT_S (K)	Forcing ($W\,m^{-2}$)	Lapse rate feedback ($W\,m^{-2}\,K^{-1}$)
'4xCO_2'	3.1	5.1	0.79
'Solar'	-1.5	-3.0	0.43
'ET'	-0.51	-1.4	-0.20
'All'	1.1	0.63	1.9

Table 1. Values for ΔT_S, forcing and lapse rate feedback for each temperature change structure of the single column model of the polar atmosphere (figure 2b).

We calculate the forcing on the high latitude atmospheric column for each simulation by calculating the change in outgoing longwave radiation (OLR) induced by the changes in surface and tropospheric temperature (here, the tropopause is set at 200 hPa). The temperature kernel of the column model is calculated by separately increasing the surface and each pressure level by 1K and calculating the resulting OLR increase (see supplementary figure S7 for kernel structure). The total feedback determines the surface temperature change per unit of forcing and is decomposed into the Planck, lapse rate, and water vapor feedbacks. The change in water vapor is small and induces a negligible change in surface temperature, hence it is ignored in the main text (see supplementary figure S8). The Planck feedback is computed as the OLR change from a 1K temperature increase at the surface and in the troposphere. Its value is -2.6 $W\,m^{-2}\,K^{-1}$, which is comparable to comprehensive GCM estimates in high latitudes[3]. The temperature feedback is computed as the OLR increase induced by the surface and tropospheric temperature change divided by the surface temperature change, and the lapse rate feedback as the temperature feedback minus the Planck feedback. The lapse rate feedback of the "All" experiment is 1.9 $W\,m^{-2}\,K^{-1}$, which is comparable to the high latitude lapse rate feedback of the idealized GCM SRM experiment computed using aquaplanet temperature kernels[4] (not shown).

The forcing and lapse rate feedback associated with each simulation are shown in table 1. There is a 2.1 $W\,m^{-2}$ positive TOA forcing from the difference between the CO_2 and solar forcings, and a -1.4 $W\,m^{-2}$ reduction in atmospheric energy transport convergence (comparable to the change in high latitude convergence of atmospheric energy trans-

port in the idealized GCM). The relatively large surface temperature response in the "All" experiment (1.1K) for a small forcing (0.63 $\mathrm{W\,m^{-2}}$ if the change in atmospheric energy transport is considered as a forcing on the high latitude column) can be attributed to the very destabilizing lapse rate feedback (1.9 $\mathrm{W\,m^{-2}\,K^{-1}}$). If we use the CO_2 lapse rate feedback (0.79 $\mathrm{W\,m^{-2}\,K^{-1}}$), then the surface temperature change would be 0.4K instead of 1.1K. We are thus left with explaining this very destabilizing lapse rate feedback that provokes most of the residual polar warming in SRM simulations.

As shown in figure 2b, the vertical structure of temperature change in the "All" experiment can be decomposed into the effect of individual forcings and feedbacks. The warming from the increase in CO_2 is very bottom-heavy (0.79 $\mathrm{W\,m^{-2}\,K^{-1}}$ lapse rate feedback), whereas the cooling from changes in insolation and energy transport are more vertically homogeneous. When this vertically homogeneous cooling is superimposed on the bottom-heavy warming from CO_2, it decreases the OLR faster than it decreases the surface temperature. The vertical gradient in temperature is almost left unchanged (compare "CO_2" and "All" in figure 2b), the forcing on the atmospheric column is small, and the surface temperature change is 1.1K. Given the importance of the lapse rate changes between forcing agents, we turn to a more idealized SCM to develop a theoretical understanding of forcing dependence of high latitude lapse rate response.

The analytical model of the high latitude atmosphere in radiative-advective equilibrium [2] was used to show the forcing dependence of high latitude lapse rate changes. In their model, an increase in greenhouse gases leads to a more bottom-heavy temperature change than an increase in atmospheric or surface forcing. Details including the climatological temperature and temperature changes of the analytical radiative-advective model are reproduced from Cronin & Jansen [2] in text S2.

The essence of the mechanism for the forcing dependence of the high latitude lapse rate change is contained in the radiative equilibrium limit (no advection), so we discuss this simpler case. It is well understood that an atmosphere in pure radiative equilibrium is statically unstable, however the argument for the perturbation temperature is fundamentally the same as for an atmosphere in radiative-advective equilibrium and easier to understand. In this model, increasing the total longwave optical depth is analogous to increasing atmospheric CO_2, and decreasing the surface forcing is analogous to decreasing the TOA insolation (atmospheric absorption of solar radiation is ignored).

Figure 3a shows the climatological polar temperature in the pure radiative equilibrium case. Figure 3b shows the temperature change from increasing the total longwave optical depth (red) and from decreasing the surface forcing (yellow). The total longwave optical depth is increased from 3 to 3.2 and induces an instantaneous reduction in OLR by 3.6 $\mathrm{W\,m^{-2}}$, which we use for the magnitude of the reduction in surface forcing. The vertical structure of temperature change is more bottom-heavy for an increase in longwave optical depth ("CO_2", red) than for a decrease in surface forcing ("Solar", yellow). The forcing dependence of the lapse rate feedback thus does not depend on the presence of atmospheric energy transport convergence.

To explain this forcing dependence, we derive a simple expression for the temperature structure of the polar troposphere from the two-stream Schwartzchild equations for gray radiative transfer (equations 1 and 2 in text S2) with the simplifications described in Methods:

$$2\sigma T(p)^4 = F_S[1+\tau(p)] = F_S\left[1+\tau_0\left(\frac{p}{p_0}\right)^2\right],$$

where F_S is the surface forcing, τ_0 the total longwave optical depth, p the pressure and p_0 the surface pressure. This equation shows that temperatures must change at all levels for a change in F_S, but they do not change as p goes to zero for a change in τ_0.

Figure 3c shows the difference in $2\sigma T^4$ from changes in τ_0 and F_S. When τ_0 is increased from 3 to 3.2, the change in $2\sigma T^4$ is zero at the TOA and $\delta\tau_0 F_S$ at the surface. When F_S is reduced from 120 W m^{-2} to 116.4 W m^{-2}, the change in $2\sigma T^4$ is δF_S at the TOA and $\delta F_S(1+\tau_0)$ at the surface. Physically, an increase in greenhouse gases corresponds to a deepening of the atmosphere with respect to optical depth and the longwave radiative flux at the TOA is not affected; whereas a change in solar insolation affects the longwave radiative flux from the surface to the TOA. This reasoning applies for an atmosphere in pure radiative equilibrium, as well as an atmosphere in radiative-advective equilibrium (see figure S9 for an analog of figure 3 for an atmosphere in radiative-advective equilibrium).

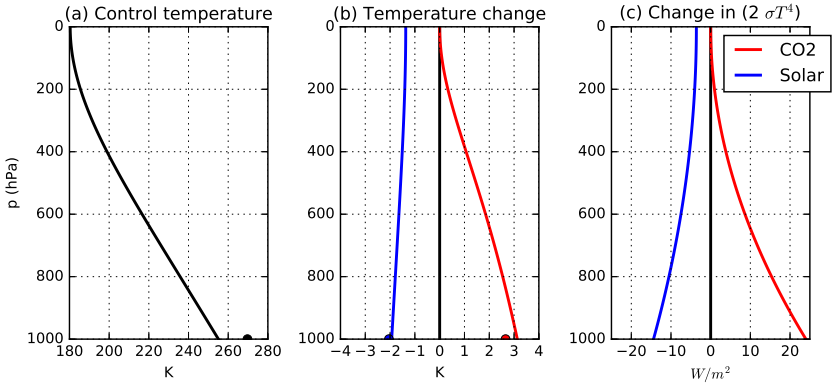

Figure 3. A pure radiative version of an analytical model of the high-latitude atmosphere captures the forcing dependence of lapse rate changes[2]. (a) Climatological temperature with no atmospheric forcing and a 120 W m^{-2} surface forcing (F_S). (b) Temperature change from increasing the total longwave optical depth by 0.2 ('CO_2', red) and from decreasing the surface forcing by 3.6 W m^{-2} ('Solar', yellow), which is equal to the instantaneous reduction in OLR from increasing the total longwave optical depth by 0.2. (c) Change in $2\sigma T^4$ for both perturbation experiments.

The high latitudes are close to radiative-advective equilibrium: the cooling from radiation is balanced by warming from atmospheric energy transport convergence. Where there is convection, the temperature of the atmospheric column can be approximated based on the surface temperature and relative humidity. Without convection, each forcing and feedback induces a different lapse rate response. In the SRM experiment, the latitudinal structure of the forcing is such that the high latitudes have a positive TOA radiative forcing and a reduction in atmospheric energy transport convergence. If we consider the atmospheric energy transport convergence as a forcing on the high latitude column, then the positive TOA forcing and reduction in atmospheric transport convergence add up to give a small forcing. However, the surface temperature change is relatively large, which is explained by a destabilizing lapse rate feedback. The vertical structure of the high latitude temperature change of an idealized GCM is decomposed using a SCM. It is shown that the warming from CO_2 alone is very bottom-heavy whereas the cooling from a reduction in insolation and atmospheric energy transport are more vertically homogeneous. The combination of a bottom-heavy warming and a vertically homogeneous cooling gives a small forcing for a relatively large surface warming. Using the no advection limit of an analytical model of the high latitude atmosphere in radiative-advective equilibrium[2], we show that the difference in the vertical structure of temperature changes from increasing CO_2 and decreasing insolation result from different changes in the boundary conditions of the radiative flux. The increase in CO_2 deepens the atmosphere with

respect to optical depth, whereas the change in insolation modifies the resulting longwave radiative fluxes through the whole atmosphere (surface to TOA). The dominance of the forcing agent dependence of lapse rate changes in provoking residual polar warming in SRM simulations can be assessed by replacing the lapse rate feedback with that of CO_2 (table 1) or considering models without this feedback [15], both of which substantially underestimate the polar warming. A major implication of the lapse rate dependence on forcing agent is that there will be residual polar surface warming even if the spatial distribution of scattering aerosols can be optimized to perfectly offset the local greenhouse gas forcing.

Methods

Idealized atmospheric general circulation model.

We use a Geophysical Fluid Dynamics Laboratory (GFDL) atmospheric general circulation model (GCM) in a configuration similar to the setup in Merlis et al. [16] and to the Model of an Idealized Moist Atmosphere (MiMA) [10]. Both setups are similar to the moist idealized GCM described in Frierson et al. (2006) but uses comprehensive radiation instead of gray radiation. In the MiMA setup, there are no clouds hence the surface albedo is uniformly increased to compensate for the cooling effect of clouds. In Merlis et al. [16], a cloud distribution is prescribed instead of being interactive. In our simulations, there are no clouds and we set the surface albedo to a hemispherically symmetric analytic distribution similar to Earth's northern hemisphere TOA albedo (see figure S1), in order to have a more realistic surface temperature gradient. Figure S2a shows the atmospheric temperature for the control simulation and it compares well with Earth's climate. We briefly describe the physical processes in the model below.

The surface boundary condition is an aquaplanet with a slab mixed layer ocean with the heat capacity of 1m of water and no representation of ocean heat transport. The GCM's spectral dynamical core has T42 spectral truncation for a nominal horizontal resolution of 2.8° x 2.8° and 30 vertical levels. The skin temperature is interactively computed using the surface radiative and turbulent fluxes, which are determined by bulk aerodynamic formulae. A k-profile scheme with a dynamically determined boundary layer height is used to parametrize the boundary layer turbulence. The GCM uses a simplified Betts-Miller convection scheme [5]. The large scale condensation is parameterized such that the relative humidity does not exceed one and the condensed water is assumed to immediately return to the surface. The model uses the comprehensive radiation scheme described in Anderson et al. [1] with annual mean solar insolation and a solar constant equal to 1365 $\mathrm{W\,m^{-2}}$. The surface has no representation of sea ice other than the surface albedo distribution, hence there is no surface albedo feedback. All simulations are run for 6000 days with time averages over the last 3000 days shown, when all climate states have reached a statistical steady state.

We perform four simulations with this model setup. The control simulation has 300ppm of CO_2 and a 1365 $\mathrm{W\,m^{-2}}$ solar constant. The increased CO_2 simulation has 1200ppm of CO_2. The reduced solar constant experiment has a 1317 $\mathrm{W\,m^{-2}}$ solar constant. The solar radiation management experiment has both increased CO_2 and a reduced solar constant. The value for the reduced solar constant was determined in order to get near-zero global surface air temperature change. Figure S2b shows the temperature difference between the control and increased CO_2 simulation and figure S2c shows the temperature difference between the control and decreased solar constant simulation. Theres a 10% deviation from linear superposition when compared to the solar radiation management experiment's temperature change, without a significant effect on the pattern of surface temperature change.

Single Column Model.

In the single column model of the high latitude atmosphere, the surface albedo, control insolation, and reduction in insolation are set such that the upwelling and downwelling TOA shortwave radiation match the idealized GCM simulations (control and SRM) poleward of 80°. Results were unchanged for a latitude bound set at 60° (see supplementary figures S5 and S6). Vertical advection is not included in the SCM, but the insensitivity of results to the latitudinal bound suggests that this does not affect our SCM-based attribution. A summary of the specific parameter settings for each run are given in the supplementary table S1.

Analytical model of high-latitude atmosphere.

The pure radiative equilibrium version of the Cronin & Jansen [2] analytic model of the high-latitude atmosphere has the convergence of atmospheric energy transport imposed at the surface to keep the temperatures similar to high latitudes. The parameters are $F_S = 120\ \mathrm{W\,m^{-2}}$, $F_A = 0\ \mathrm{W\,m^{-2}}$ and $\tau_0 = 3$, where F_S is the surface forcing, F_A the atmospheric forcing and τ_0 the total longwave optical depth.

In order to further simplify the calculations, we do not include an atmospheric window which is a strong assumption given that the column model presented in section 3 has a high value for the surface temperature kernel, suggesting a somewhat transparent atmosphere. And, the optical depth distribution with respect to pressure is also implicit within the model: the optical depth decays as the square of the pressure normalized by the surface pressure (n=2 in Cronin & Jansen [2]).

References

[1] Anderson, J. L., Balaji, V., Broccoli, A. J., Cooke, W. F., Delworth, T. L., Dixon, K. W., ... others (2004). The new GFDL global atmosphere and land model am2–lm2: Evaluation with prescribed sst simulations. *Journal of Climate*, *17*(24), 4641–4673.

[2] Cronin, T. W., & Jansen, M. F. (2016). Analytic radiative-advective equilibrium as a model for high-latitude climate. *Geophysical Research Letters*, *43*(1), 449–457.

[3] Feldl, N., & Bordoni, S. (2016). Characterizing the Hadley circulation response through regional climate feedbacks. *J. Climate*, *29*(2), 613–622.

[4] Feldl, N., Bordoni, S., & Merlis, T. M. (2017). Coupled high-latitude climate feedbacks and their impact on atmospheric heat transport. *Journal of Climate*, *30*(1), 189–201.

[5] Frierson, D. M. (2007). The dynamics of idealized convection schemes and their effect on the zonally averaged tropical circulation. *J. Atmos. Sci.*, *64*(6), 1959–1976.

[6] Govindasamy, B., & Caldeira, K. (2000). Geoengineering Earth's radiation balance to mitigate CO_2-induced climate change. *Geophys. Res. Lett.*, *27*, 2141–2144.

[7] Hansen, J., Sato, M., & Ruedy, R. (1997). Radiative forcing and climate response. *Journal of Geophysical Research: Atmospheres*, *102*(D6), 6831–6864.

[8] Henry, M., & Merlis, T. M. (2019). The role of the nonlinearity of the stefan–boltzmann law on the structure of radiatively forced temperature change. *Journal of Climate*, *32*(2), 335–348.

[9] Huang, Y., Tan, X., & Xia, Y. (2016). Inhomogeneous radiative forcing of homogeneous greenhouse gases. *J. Geophys. Res.: Atmospheres*, *121*(6), 2780–2789.

[10] Jucker, M., & Gerber, E. (2017). Untangling the annual cycle of the tropical tropopause layer with an idealized moist model. *Journal of Climate*, *30*(18),

7339–7358.

[11] Kalidindi, S., Bala, G., Modak, A., & Caldeira, K. (2015). Modeling of solar radiation management: a comparison of simulations using reduced solar constant and stratospheric sulphate aerosols. *Climate Dynamics*, *44*(9-10), 2909–2925.

[12] Kravitz, B., Robock, A., Boucher, O., Schmidt, H., Taylor, K. E., Stenchikov, G., & Schulz, M. (2011). The geoengineering model intercomparison project (GeoMIP). *Atmospheric Science Letters*, *12*(2), 162–167.

[13] Laliberté, F., & Kushner, P. (2013). Isentropic constraints by midlatitude surface warming on the Arctic midtroposphere. *Geophysical Research Letters*, *40*(3), 606–611.

[14] Manabe, S., & Wetherald, R. T. (1975). The effects of doubling the CO_2 concentration on the climate of a general circulation model. *J. Atmos. Sci.*, *32*, 3–15.

[15] Merlis, T. M., & Henry, M. (2018). Simple estimates of polar amplification in moist diffusive energy balance models. *Journal of Climate*(2018).

[16] Merlis, T. M., Schneider, T., Bordoni, S., & Eisenman, I. (2013). Hadley circulation response to orbital precession. Part I: Aquaplanets. *J. Climate*, *26*, 740–753.

[17] Pithan, F., & Mauritsen, T. (2014). Arctic amplification dominated by temperature feedbacks in contemporary climate models. *Nat. Geosci.*, *7*, 181–184.

[18] Rose, B. E. (2018). Climlab: A python toolkit for interactive, processoriented climate modeling. *J. Open Source Software*, *3*(24), 659.

[19] Russotto, R. D., & Ackerman, T. P. (2018). Energy transport, polar amplification, and ITCZ shifts in the GeoMIP G1 ensemble. *Atmospheric Chemistry and Physics*, *18*(3), 2287–2305.

[20] Stocker, T. F., et al. (Eds.). (2013). *Climate change 2013: The physical science basis*. Cambridge and New York: Cambridge University Press.

[21] Xu, K.-M., & Emanuel, K. A. (1989). Is the tropical atmosphere conditionally unstable? *Monthly Weather Review*, *117*(7), 1471–1479.

Acknowledgments

This work was supported by Fonds de Recherche du Québec — Nature et Technologies (FRQNT) Nouveau Chercheur award, a Natural Sciences and Research Council (NSERC) Discovery grant, and a Compute Canada allocation. We acknowledge Brian Rose's help in setting up the single column model by adding an external forcing term.

Author contributions

M.H. designed the study, conducted the model experiments and wrote the initial manuscript draft. T.M. contributed to the interpretation of the results and improvement of the manuscript.

Data availability

All the code and data are publically available at https://github.com/matthewjhenry/HM19_SRM